# Modulation of SF3B1 in the pre-mRNA spliceosome induces a RIG-I-dependent type I IFN response

Received for publication, December 9, 2020, and in revised form, September 22, 2021 Published, Papers in Press, October 5, 2021,
https://doi.org/10.1016/j.jbc.2021.101277

**Aaron Y. Chang[1], Yu Jerry Zhou[1], Sharanya Iyengar[2], Piotr W. Pobiarzyn[1], Pavel Tishchenko[1], Kesha M. Shah[1], Heather Wheeler[3], Yue-Ming Wang[3], Paula M. Loria[3], Frank Loganzo[1], and Seng-Ryong Woo[1,*]**

*From the [1]Oncology Research & Development, Pfizer Inc, Pearl River, and [2]Emerging Science & Innovation, Pfizer Inc, Pearl River, New York, USA; [3]Medicine Design, Worldwide Research & Development, Pfizer Inc, Groton, Connecticut, USA*

Edited by Karin Musier-Forsyth

**Nucleic acid–sensing pathways play critical roles in innate immune activation through the production of type I interferon (IFN-I) and proinflammatory cytokines. These factors are required for effective antitumor immune responses. Pharmacological modulators of the pre-mRNA spliceosome splicing factor 3b subunit 1 (SF3B1) are under clinical investigation as cancer cytotoxic agents. However, potential roles of these agents in aberrant RNA generation and subsequent RNA-sensing pathway activation have not been studied. In this study, we observed that SF3B1 pharmacological modulation using pladienolide B (Plad B) induces production of aberrant RNA species and robust IFN-I responses *via* engagement of the dsRNA sensor retinoic acid–inducible gene I (RIG-I) and downstream interferon regulatory factor 3. We found that Plad B synergized with canonical RIG-I agonism to induce the IFN-I response. In addition, Plad B induced NF-κB responses and secretion of proinflammatory cytokines and chemokines. Finally, we showed that cancer cells bearing the hotspot SF3B1$^{K700E}$ mutation, which leads to global aberrant splicing, had enhanced IFN-I response to canonical RIG-I agonism. Together, these results demonstrate that pharmacological modulation of SF3B1 in cancer cells can induce an enhanced IFN-I response dependent on RIG-I expression. The study suggests that spliceosome modulation may not only induce direct cancer cell cytotoxicity but also initiate an innate immune response *via* activation of RNA-sensing pathways.**

Nucleic acid–sensing pathways play a critical role in innate immune activation against viral infections and cancers (1, 2). Activation of these pathways induces production of type I interferons (IFN-I) and other proinflammatory cytokines. In cancer, these pathways can be activated by sensing aberrant self-nucleic acid species and promote antitumor immune responses (2). While aberrant cytoplasmic DNA can be preferentially sensed through the cyclic GMP–AMP synthase–stimulator of interferon genes (STING) pathway (2), cytoplasmic RNA species can be recognized by retinoic acid–inducible gene I (RIG-I) and/or melanoma differentiation–associated protein 5 (MDA5) (3, 4). RIG-I activation *via* cytoplasmic dsRNA induces IFN-I production and promotes apoptosis and pyroptosis (1, 5). Canonical RIG-I activation requires the downstream adaptor protein MAVS (mitochondrial antiviral signaling protein), which ultimately leads to activation of interferon regulatory factor 3 (IRF3), a key transcription factor that promotes IFN-I production (1). Interestingly, tumor cell–intrinsic RIG-I expression seems to be required for optimal checkpoint blockade therapy against cytotoxic T-lymphocyte–associated protein 4 (6) in mouse tumor models. Consistently, RIG-I agonism was suggested to be an effective cancer immunotherapy (6).

It has been reported that DNA damage inducers (DNA-damaging agents, ionizing radiation, and DNA damage response inhibitors) can activate tumor-intrinsic STING and IFN-I responses *via* exposure of cytoplasmic DNA (7–9). However, it is unknown whether therapeutically targeting RNA-processing mechanisms would activate RNA-sensing pathways to induce subsequent IFN-I production. Recent studies have illustrated that tumor-intrinsic loss of RNA-editing function can substantially increase the inflammation and immunogenicity of a tumor. For example, genetic loss of adenosine deaminase acting on RNA 1–mediated A-I editing leads to aberrant RNA sensing by protein kinase R and MDA5 (10, 11). This leads to tumor inflammation, growth inhibition, and overcomes resistance to immune checkpoint blockade in mouse tumor models. Along with this observation, normal N6-methyladenosine modification has been suggested to be a marker of "self" circular RNA and prevents activation of RIG-I by these species. Indeed, unedited RNA can readily activate RIG-I in biochemical assays, but N6-methyladenosine modification of the RNA prevents RIG-I activation (12). Thus, there is biochemical and genetic evidence that certain aberrantly processed self-RNA species can stimulate RNA-sensor activation and induce subsequent immune responses.

* For correspondence: Seng-Ryong Woo, realwoomir@gmail.com.
Present address for Aaron Y Chang: Regeneron Pharmaceuticals, Tarrytown, NY, USA.
Present address for Sharanya Iyengar: Merck & Co, Inc, Boston, MA, USA.
Present address for Piotr W. Pobiarzyn: HiberCell, New York, NY, USA.
Present address for Pavel Tishchenko: Gotham Therapeutics, New York, NY, USA.
Present address for Frank Loganzo: Regeneron Pharmaceuticals, Tarrytown, NY, USA.
Present address for Seng-Ryong Woo: AbbVie, North Chicago, IL, USA.



© 2021 THE AUTHORS. Published by Elsevier Inc on behalf of American Society for Biochemistry and Molecular Biology. This is an open access article under the CC BY-NC-ND license (http://creativecommons.org/licenses/by-nc-nd/4.0/).

The spliceosome is a nucleoprotein complex that functions to remove introns from eukaryotic pre-mRNA (13–15). The enzymatic process of mRNA splicing is complex and highly regulated (15). Splicing dysregulation is a hallmark of cancer, and aberrant splicing is enriched in cancer cells compared with healthy tissue (13, 15). Recurrent mutations are found on the spliceosome splicing factor 3b subunit 1 (SF3B1) and lead to global alternative splicing (16, 17). These SF3B1 change-of-function mutations are found in large portions of cancers (approximately 6–26% of chronic lymphocytic leukemia, 15–29% of uveal melanomas, and 2–4% of breast tumors (18)) and have been associated with both poor and favorable prognosis depending on the context and tumor type.

In addition, SF3B1 pharmacological modulators are being studied as potent anticancer agents and have progressed to clinical trials. SF3B1 modulators can control tumors effectively in mouse models (19–21), and one agent that has progressed to phase I trials (H3-8800) exhibits preferential cytotoxicity to cells bearing the common SF3B1$^{K700E}$ mutation (20). SF3B1 modulators such as pladienolide B (Plad B) or spliceostatins (22) do not simply arrest splicing but rather modulate splicing through alternative branch point usage (23, 24). Indeed, the functional outcomes of spliceosome modulators do not fully overlap with loss of function through siRNA (25). They therefore can generate aberrant RNA species such as back-spliced circular RNA (26), retained introns (19), or alternative splice products (27). Although SF3B1 modulators induce direct cancer cell cytotoxicity, it is unknown if they can induce aberrant RNA species that activate innate immune signaling pathways. We hypothesize that spliceosome modulation generates aberrant dsRNA species leading to RNA sensor–mediated IFN-I production and a potentially enhanced anti-tumor immune response.

In this study, we demonstrate that specific SF3B1 pharmacological modulation induces IFN-I responses dependent on RIG-I. In addition, we illustrate that SF3B1$^{K700E}$-mutant cancer cells stimulated with RIG-I agonists produce enhanced levels of IFN-I. Together, the study demonstrates how spliceosome dysfunction can evoke nucleic acid–sensing pathways for immune activation.

## Results

### SF3B1 pharmacological modulation induces IFN-I and NF-κB responses

To determine whether spliceosome modulation induces IFN-I responses, we utilized a reporter lung adenocarcinoma cell line A549-Dual expressing luciferase under the promoter of interferon-stimulated gene 54 (ISG54) and a secreted embryonic alkaline phosphatase (SEAP) reporter gene under the control of NF-κB. Treatment for 24 h with SF3B1 modulators Plad B or spliceostatin derivative PF-06437837 (28) induced robust ISG responses as measured by luciferase activity (Fig. 1*A*). At this time point, viability was minimally affected (Fig. 1*A*). It is possible that IFN-I responses are caused by general cell stress. However, other cytotoxic agents such as a DNA-damaging agent (SN38) or endoplasmic reticulum–stress inducer (thapsigargin) did not induce substantial IFN-I responses at 24 and 72 h, suggesting that Plad B-induced IFN-I was not because of general cell stress but rather through SF3B1 modulation (Fig. S1*A*). To ensure functional modulation of SF3B1, we used an intron-retention PCR assay to determine the relative levels of spliced and unspliced transcripts from two published genes (*DNAJB1* and *RIOK3*) (19) after 18 h of Plad B treatment (Fig. 1*B*). Indeed, we observed a dose-dependent level of intron retention that correlated with substantial IFN-β and ISG54 transcript expression. We verified that our findings were broadly applicable by treating several additional tumor cell lines with SF3B1 modulators. Murine tumor cell lines B16F10, CT26, EMT6, MC38, and 4T1 induced different levels of detectable IFN-β after Plad B treatment (Fig. 1, *C* and *D*). B16F10 produced the highest levels of IFN-β in response to Plad B. To prove that Plad B-mediated IFN-I induction was due to on-target SF3B1 modulation, we generated a B16F10-SF3B1$^{R1074H}$ mutant cell line. The SF3B1$^{R1074H}$ mutation prevents Plad B binding to SF3B1 and confers resistance to cytotoxic effects (23, 24, 29). B16F10-SF3B1$^{R1074H}$ cells were resistant to Plad B cytotoxicity and did not produce IFN-β suggesting that specific binding of Plad B to SF3B1 was largely responsible for IFN-I production (Fig. 1*E*). To determine whether spliceosome modulation also induces NF-κB responses, we utilized a NF-κB SEAP reporter assay in A549-Dual cells. Plad B induced substantial NF-κB activity as measured by SEAP activity (Fig. 2*A*). The response was comparable to treatment with tumor necrosis factor alpha (TNFα) or the RIG-I agonist (3p-hpRNA; hairpin RNA [hpRNA]). In addition, B16F10 cells treated with Plad B secreted substantial amounts of the NF-κB–associated C-X-C motif chemokine ligand 1 and C-X-C motif chemokine ligand 10 (Fig. 2*B*). C-X-C motif chemokine ligand 10 has been reported as a chemoattractant for tumor-infiltrating lymphocytes (30, 31). Consistently, A549-Dual cells treated with Plad B secreted detectable levels of NF-κB–associated cytokines interleukin 6 (IL)-6, IL-8, and minimal TNFα (Fig. S1*C*). Together, the data suggest that SF3B1 modulators induce IFN-I and NF-κB responses in a range of tumor cell lines.

### SF3B1 modulator–induced IFN-I response is dependent on RIG-I expression

The ability of SF3B1 modulators to induce an IFN-I response, or a mechanism to do so, has not been reported thus far. We hypothesized that SF3B1 modulation induces cytoplasmic aberrant RNA species that bind innate RNA sensors and initiate IFN-I responses. To test this, we utilized commercially available A549-Dual sublines with genetic deletions of key RNA sensors MDA-5 and RIG-I. Whereas deletion of MDA5 had no effect, RIG-I deletion largely abrogated IFN-I response to Plad B (Fig. 3*A*). Loss of functional RIG-I was confirmed by lack of response to a RIG-I agonist (3p-hpRNA) in A549-Dual-RIG-I-KO cells (Fig. S1*B*). Response to IFN-α2 was maintained confirming the reporter function was intact (Fig. S1*B*). To further confirm that RIG-I engagement is critical for Plad B-mediated IFN-I responses,

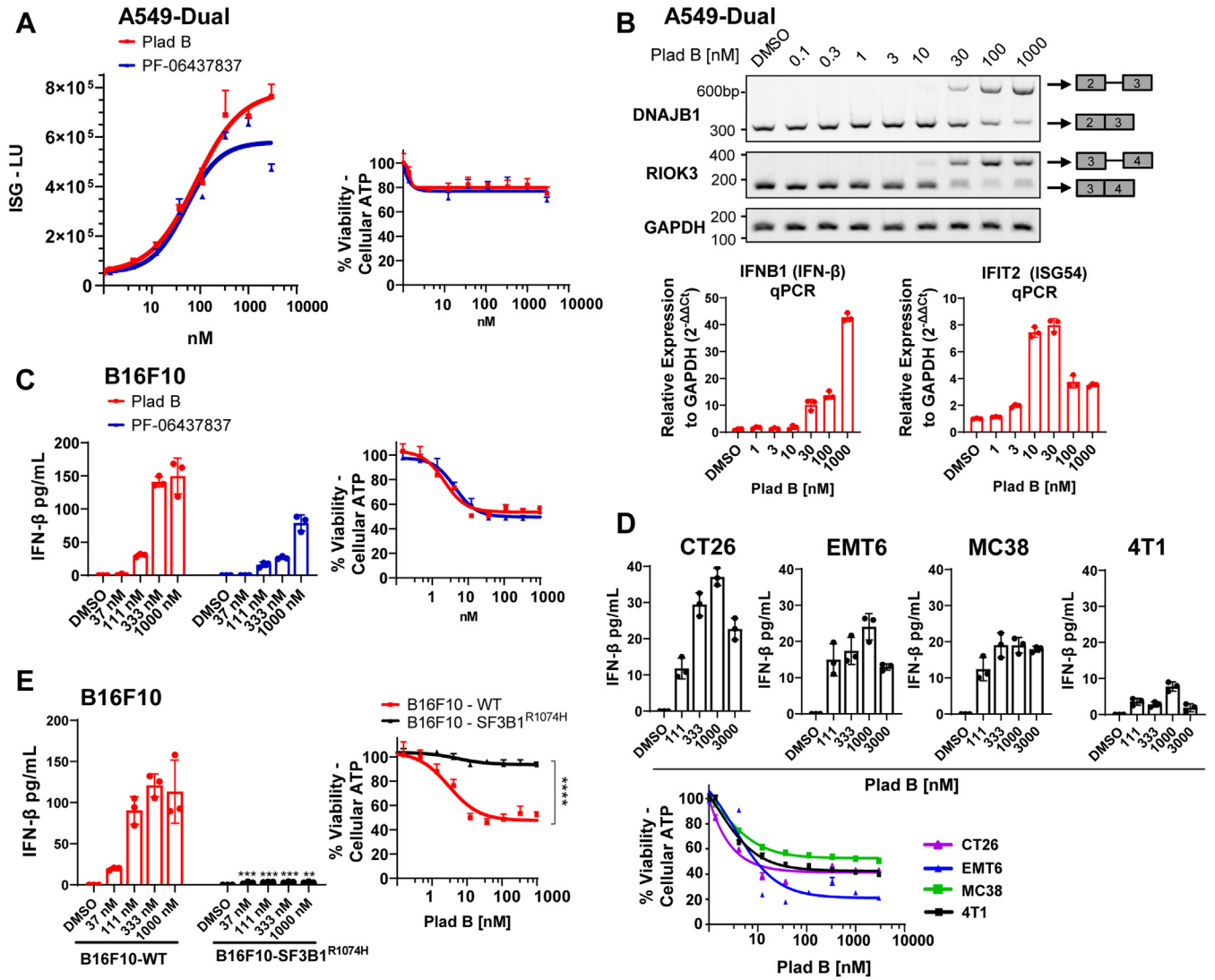


**Figure 1. SF3B1 pharmacological modulation induces IFN-I responses in tumor cells.** *A*, A549-Dual cells were treated for 24 h with Plad B or spliceostatin analog PF-06437837, and IFN-I reporter ISG-Luc activity was measured by QUANTI-Luc and raw light unit (LU) values are plotted. CellTiter-Glo was used to determine relative cell viability as calculated as a percentage of LUs *versus* control dimethyl sulfoxide–treated cells. *B*, A549-Dual cells were treated with Plad B for 18 h followed by mRNA extraction, complementary DNA synthesis, and intron-retention RT–PCR for the indicated genes with primers spanning exons. Top bands for DNAJB1 and RIOK3 indicate unspliced mRNA. GAPDH does not undergo splicing and was included as a loading control. IFNB1 (IFN-β) and IFIT2 (ISG54) transcript expression was measured by quantitative PCR. *C*, B16F10 cells were treated for 24 h with Plad B or PF-06437837, and ELISA was used to measure IFN-β in the supernatant, whereas CellTiter-Glo was used to determine relative cell viability. *D*, the indicated murine tumor lines were treated for 24 h with Plad B, and ELISA was used to quantify IFN-β in the supernatant, whereas CellTiter-Glo was used to determine relative cell viability. *E*, B16F10-SF3B1$^{R1074H}$ mutant cell line was generated using CRISPR–Cas9 gene editing. Cells were treated for 24 h with Plad B, and ELISA was used to measure IFN-β in the supernatant, whereas CellTiter-Glo was used to determine relative cell viability. Statistical analyses were performed using the unpaired parametric *t* test comparing experimental samples to the relevant dose in control cells where indicated, with *p* values <0.05 considered significant (*$p < 0.05$; **$p < 0.01$; ***$p < 0.001$; and ****$p < 0.0001$). All data are representative of n = 3 experiments. IFN-I, type I interferon; Plad B, pladienolide B; SF3B1, spliceosome splicing factor 3b subunit 1.

we generated RIG-I-KO clones from the murine cell lines B16F10 and CT26 using the CRISPR–Cas9 system. Successful KO of RIG-I was confirmed by Western blot analysis and functional assays after treatment with 3p-hpRNA (Fig. S2, *A* and *B*). Indeed, RIG-I deletion in both B16F10 and CT26 substantially reduced Plad B-mediated IFN-β secretion (Fig. 3*B*). The human embryonic kidney (HEK)-Lucia Null reporter line is deficient for endogenous RIG-I expression and showed minimal IFN-I response to Plad B treatment (Fig. 3*C*). However, HEK-Lucia RIG-I (reconstituted RIG-I expression in the background of HEK-Null) potentiated an IFN-I response to Plad B, further confirming that RIG-I was crucial for the SF3B1 modulator–induced IFN-I response. Consistently, when A549-Dual-RIG-I-KO cells (A549-RIG-I-KO) were reconstituted with RIG-I protein by lentiviral transduction (A549-RIG-I-Recon), the ability to generate an IFN-I response to Plad B was enhanced *versus* A549-RIG-I-KO (Fig. 3*D*). RIG-I loss did not affect the HEK-Lucia, CT26, or A549-Dual cell viability after Plad B treatment suggesting that RIG-I signaling was not necessary for direct cytotoxic effects of Plad B (Fig. S3*A*). The collective data demonstrate that RIG-I is required for SF3B1 modulator–induced IFN-I responses.

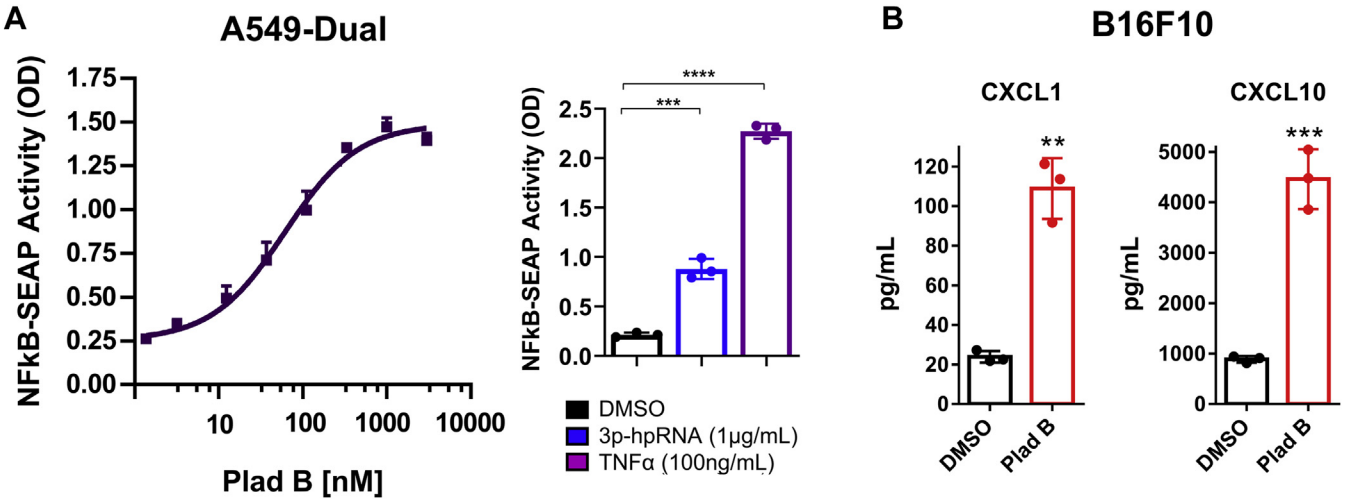


**Figure 2. SF3B1 pharmacological modulation induces NF-κB response and secretion of CXCL1 and CXCL10 chemokines.** *A*, A549-Dual cells were treated with increasing doses of Plad B for 24 h before NF-κB–SEAP response was measured using QUANTI-Blue. Saturating doses of 3p-hpRNA and TNFα were included as positive controls, and absorbance values are plotted. Data are representative of n = 3 experiments. *B*, B16F10 cells were treated for 24 h with 333 nM Plad B before CXCL1 and CXCL10 in supernatant was measured by Luminex multiplex cytokine assay. Statistical analyses were performed using the unpaired parametric *t* test comparing the experimental sample to control cells where indicated. *p* Values <0.05 were considered significant (*$p < 0.05$; **$p < 0.01$; ***$p < 0.001$; and ****$p < 0.0001$). Data are representative of n = 3 experiments (*A*) and n = 2 experiments (*B*). CXCL1, C-X-C motif chemokine ligand 1; CXCL10, C-X-C motif chemokine ligand 10; hpRNA, hairpin RNA; Plad B, pladienolide B; SEAP, secreted embryonic alkaline phosphatase; SF3B1, spliceosome splicing factor 3b subunit 1; TNFα, tumor necrosis factor alpha.

### *SF3B1 modulator–induced IFN-I response is dependent on IRF3*

Next, we investigated downstream signaling pathways to further elucidate how IFN-I responses were generated after SF3B1 modulation. IRF3 is a key transcription factor downstream of RIG-I that can promote IFN-β production (1). To determine whether IRF3 is required for Plad B-induced IFN-I responses, we knocked down IRF3 expression in A549-Dual reporter cells using siRNA before treatment with Plad B. We observed a substantial decrease of IFN-I responses in IRF3 knockdown cells (Fig. 4*A*) demonstrating that IRF3 is a key downstream factor required for the Plad B-induced IFN-I response. IRF3 dependency was also observed in THP1-Dual cells where Plad B-mediated IFN-I response was not detected in THP1-Dual-IRF3-KO cells (Fig. S3*B*). MAVS is a reported downstream adaptor protein crucial for canonical RIG-I signaling. Surprisingly, Plad B-induced IFN-I responses were largely maintained after MAVS knockdown by siRNA (Fig. 4*B*). It is possible that insufficient knockdown of MAVS by siRNA would allow maintained response. Therefore, we also tested A549-Dual-MAVS-KO cells (Invivogen) with Plad B treatment. Genetic ablation of MAVS did not abrogate the IFN-I response to Plad B, consistent with the siRNA data (Fig. 4*C*). Although we cannot rule out the possibility that a truncated MAVS allows maintained response to Plad B, A549-Dual-MAVS-KO cells have a near-completely abrogated response to the canonical RIG-I agonist 3p-hpRNA (Fig. S1*B*). Therefore, canonical MAVS functions appear to be ablated in the A549-Dual-MAVS-KO cells. A549-Dual-MAVS-KO cells maintained similar viability as their WT controls in response to Plad B suggesting that Plad B cytotoxicity did not depend on MAVS (Fig. S3*A*). As further confirmation, we generated additional clones of A549-Dual-MAVS-KO using CRISPR–Cas9 and single-guide RNAs (sgRNAs) designed to target the N-terminal region of MAVS. This strategy limits the possibility of truncated MAVS protein that still possess caspase recruitment domains. Our additional A549-Dual-MAVS-KO clones demonstrated near-completely abrogated response to the canonical RIG-I agonist 3p-hpRNA but maintained IFN-I response to Plad B (Fig. S4), consistent with the siRNA and A549-Dual-MAVS-KO (Invivogen) data. In addition, both the human monocyte-like THP1-Dual and THP1-Dual-MAVS-KO cells exhibited an IFN-I response to Plad B (Fig. S3*B*). However, the IFN-I response was lower than other cell lines tested, likely because of high sensitivity to Plad B cytotoxic effects even at 24 h. Based on these results, we conclude that the Plad B-induced IFN-I response requires RIG-I and IRF3 signaling pathways. The Plad B-induced IFN-I response may have distinct and undefined adaptor involvement compared with canonical 3p-hpRNA IFN-I responses at least in A549-Dual and THP1-Dual reporter cells.

### *Spliceosome dysfunction enhances IFN-I response to a RIG-I agonist*

The data thus far suggested that SF3B1 modulator–induced IFN-I may be distinct from canonical RIG-I activation pathway. Therefore, we sought to determine how SF3B1 modulation interacts with canonical RIG-I activation. To test this, we cotreated A549-Dual or B16F10 with increasing doses of the canonical RIG-I agonist 3p-hpRNA along with Plad B. Intriguingly, cotreatment led to strong synergy of the two compounds in inducing IFN-I responses (Figs. 5*A* and S5). This suggests that the biochemical mechanism of RIG-I engagement by Plad B can be distinct from 3p-hpRNA and that the two pathways might be cooperative instead of competitive. Cytotoxic effects of Plad B and 3p-hpRNA were not substantially additive (Figs. 5*A* and S5). The ability of a

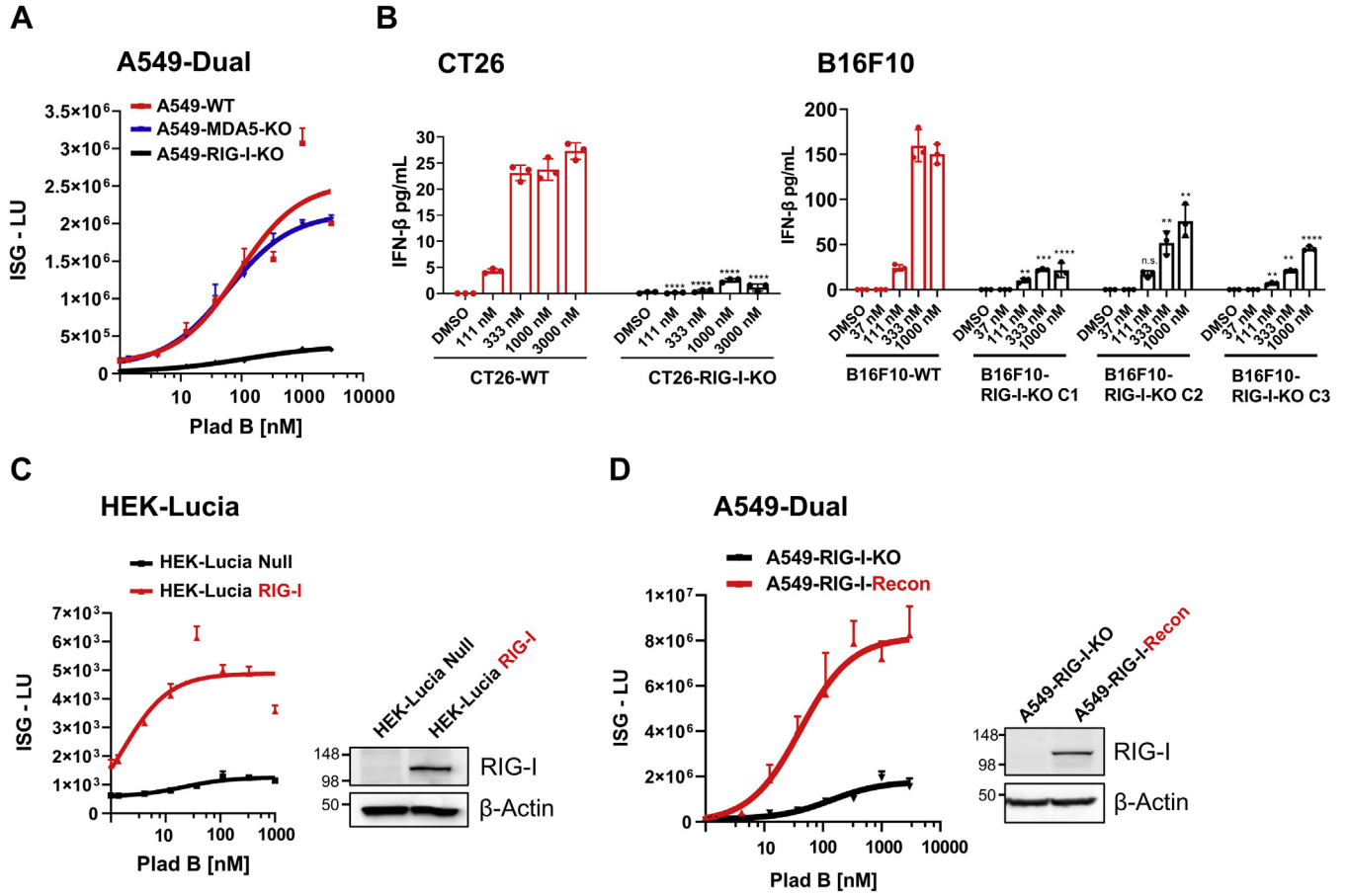


**Figure 3. SF3B1 modulator-induced IFN-I response is dependent on RIG-I.** *A*, A549-Dual-WT, A549-Dual-MDA5-KO, and A549-Dual-RIG-I-KO cells were treated with Plad B for 24 h before ISG response was measured using QUANTI-Luc, and raw light unit (LU) values are plotted. *B*, a CT26-RIG-I-KO clone and three B16F10-RIG-I-KO clones (C1, C2, and C3) were generated using CRISPR–Cas9 to genetically ablate RIG-I. Cells were treated with Plad B for 24 h, and IFN-β secretion was measured by ELISA. *C*, HEK-Lucia Null or HEK-Lucia RIG-I (RIG-I overexpressed in the background of HEK-Lucia Null) were treated with Plad B for 24 h before IFN-I response was quantified by QUANTI-Luc. Western blot analysis was used to confirm RIG-I protein overexpression. *D*, A549-Dual-RIG-I-KO cells were transduced with full-length human RIG-I. Western blot was used to confirm reconstituted expression (A549-RIG-I-Recon), and cells were treated with Plad B for 24 h before ISG response was measured using QUANTI-Luc. Statistical analyses were performed using the unpaired parametric *t* test comparing the experimental sample to the relevant dose in control cells where indicated. *p* Values <0.05 were considered significant (*$p < 0.05$; **$p < 0.01$; ***$p < 0.001$; and ****$p < 0.0001$). Immunoblots confirming RIG-I expression after transduction are representative of n = 2 experiments. All other experimental data are representative of n = 3 experiments. HEK, human embryonic kidney; IFN-I, type I interferon; ISG, interferon-stimulated gene 54; MDA5, melanoma differentiation–associated protein 5; Plad B, pladienolide B; RIG-I, retinoic acid–inducible gene I; SF3B1, spliceosome splicing factor 3b subunit 1.

canonical RIG-I agonist to synergize with Plad B led us to hypothesize that RIG-I agonists would be more effective in cancer cells that harbor spliceosome mutations resulting in basal spliceosome dysfunction. SF3B1$^{K700E}$ is one of the most common SF3B1 mutations found in various hematopoietic malignancies and breast cancers and leads to global aberrant splicing (16, 18). We thus generated SF3B1$^{K700E}$-expressing cells through lentiviral transduction with full-length SF3B1$^{K700E}$. Upon treatment with the RIG-I agonist 3p-hpRNA, B16F10-SF3B1$^{K700E}$ and 4T1-SF3B1$^{K700E}$ cells produced more IFN-β than SF3B1$^{WT}$-transduced controls (Fig. 5*B*). 3p-hpRNA-mediated cytotoxicity did not substantially depend on SF3B1$^{K700E}$ expression. Therefore, the results suggest that tumor cells bearing SF3B1$^{K700E}$ may be more sensitive to canonical RIG-I agonist–induced IFN-I responses.

## Discussion

These combined data demonstrate that SF3B1 pharmacological modulation induces robust IFN-I responses dependent on the RNA sensor RIG-I. The study expands the paradigm that aberrant self-RNA can be sensed by nucleic acid sensors that typically function as innate immune defenses. Intriguingly, the SF3B1 modulator–induced IFN-I response is mediated by RIG-I and downstream IRF3 activation but may utilize an adaptor distinct from the canonical MAVS mechanism in A549 reporter cells. Whether this distinct pathway activation is broadly observed in different cell and cancer types remains to be studied.

The first outstanding question is how does Plad B engage RIG-I activation? A logical hypothesis is that the SF3B1 modulators generate various structures of aberrant RNA, and some of these can directly bind to and activate RIG-I. One critical consideration is that not all RNA species that bind to RIG-I activate the RIG-I/IFN-I pathway. For example, while RIG-I can be stimulated by unedited RNA lacking 6-methyladenosine (12), it can also be actively antagonized by RNAs containing 5′-monophosphates (5′-p RNAs), which are abundant in healthy cells and therefore represent a gating

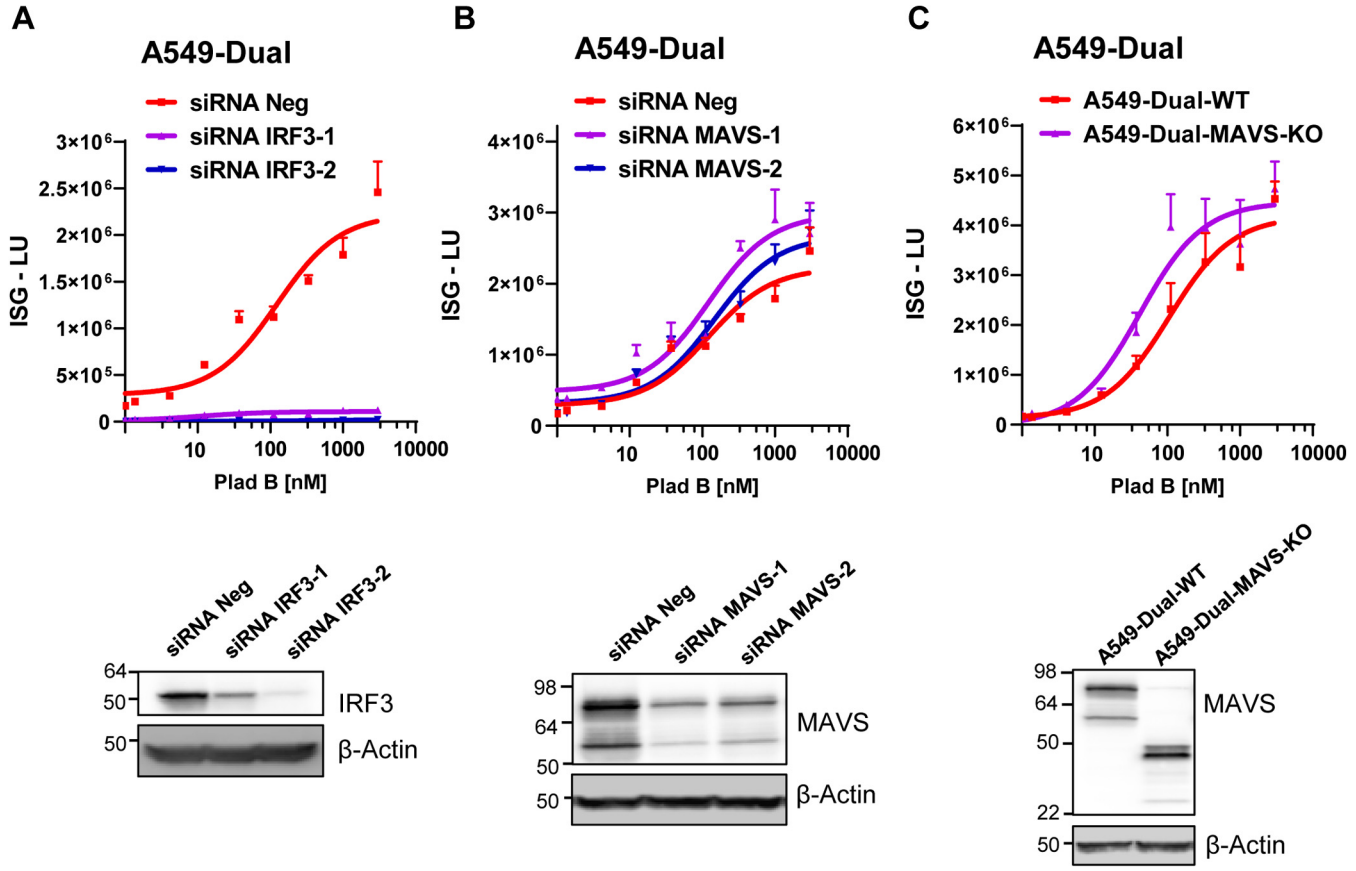


**Figure 4. SF3B1 modulator–induced IFN-I response is dependent on IRF3 but distinct from canonical MAVS activation.** siRNA against (*A*) IRF3 or (*B*) MAVS was transfected into A549-Dual cells for 72 h before confirming knockdown by immunoblot. Cells were replated and treated for 24 h with Plad B. ISG response was measured by QUANTI-Luc and a luminometer. Light unit (LU) values are plotted. *C*, A549-Dual-WT or A549-Dual-MAVS-KO cells were treated with Plad B for 24 h before ISG response was measured using QUANTI-Luc. Deletion of functional MAVS in A549-Dual-MAVS-KO was confirmed using Western blot. Detected band in A549-Dual-MAVS-KO is likely truncated and nonfunctional MAVS. All data are representative of n = 3 experiments. IFN-I, type I interferon; IRF3, interferon regulatory factor 3; ISG, interferon-stimulated gene; MAVS, mitochondrial antiviral signaling protein; SF3B1, spliceosome splicing factor 3b subunit 1.

mechanism to prevent basal activation to self-RNA species (32). The RNA-binding protein TAR DNA-binding protein 43 has also been reported to prevent accumulation of endogenous RNA species that can activate RIG-I (33). If SF3B1 modulation increases unedited RNA lacking 6-methyladenosine or in contrast decreases RNAs containing 5′-monophosphates or decreases TAR DNA-binding protein 43 expression, these can also represent mechanisms to induce RIG-I activation. Although RIG-I is generally thought to be specific for dsRNAs bearing a 5′ triphosphate or diphosphate group (32), there is increasing evidence that RIG-I can be more promiscuous than originally believed. In fact, reports have demonstrated that RIG-I can bind to circular RNA with no ends (34). SF3B1 modulation can generate back-spliced circular RNA (26), and these species represent another potential RIG-I ligand. It can also be expected that these distinct structures interact with RIG-I differently than canonical 3p-hpRNA. Distinct interactions with RIG-I may result in unique RIG-I conformational changes and differing downstream pathway activation. For example, a host-derived long noncoding RNA bound to RIG-I has been reported to promote RIG-I signaling by acting as a scaffold that directly binds and bridges RIG-I and tripartite motif containing 25 (35). It is plausible that while some Plad B-induced RNA ligands bind to RIG-I to activate signaling, others similarly act as a scaffold to enhance signaling. In conjunction, SF3B1 modulation may modify key factors involved in the RIG-I activation pathway and amplify responses to RNA species. A similar mechanism has been identified in the context of SF3B1 mutation, whereby alternatively spliced mitogen-activated protein kinase kinase kinase 7 potentiates NF-κB activation by lipopolysaccharides (36).

The second open-ended question is how can Plad B-induced IFN-I response be dependent on RIG-I expression in A549 cells but not the canonical adaptor MAVS? RIG-I pathway activation has been reported to be mediated by other adaptors such as apoptosis-associated speck-like protein containing a caspase recruitment domain for inflammatory responses (37). Similarly, other unidentified factors may function downstream of RIG-I and mediate IRF3 activation and IFN-I responses in the context of SF3B1 modulation. Importantly, SF3B1 modulation can generate alternatively spliced factors, several of which have unknown neomorphic functions. Mutations in the spliceosome component U2AF1 has been reported to generate a mis-spliced long isoform of interleukin 1 receptor–associated kinase 4 that promotes innate immune signals to NF-κB (38). Such studies highlight

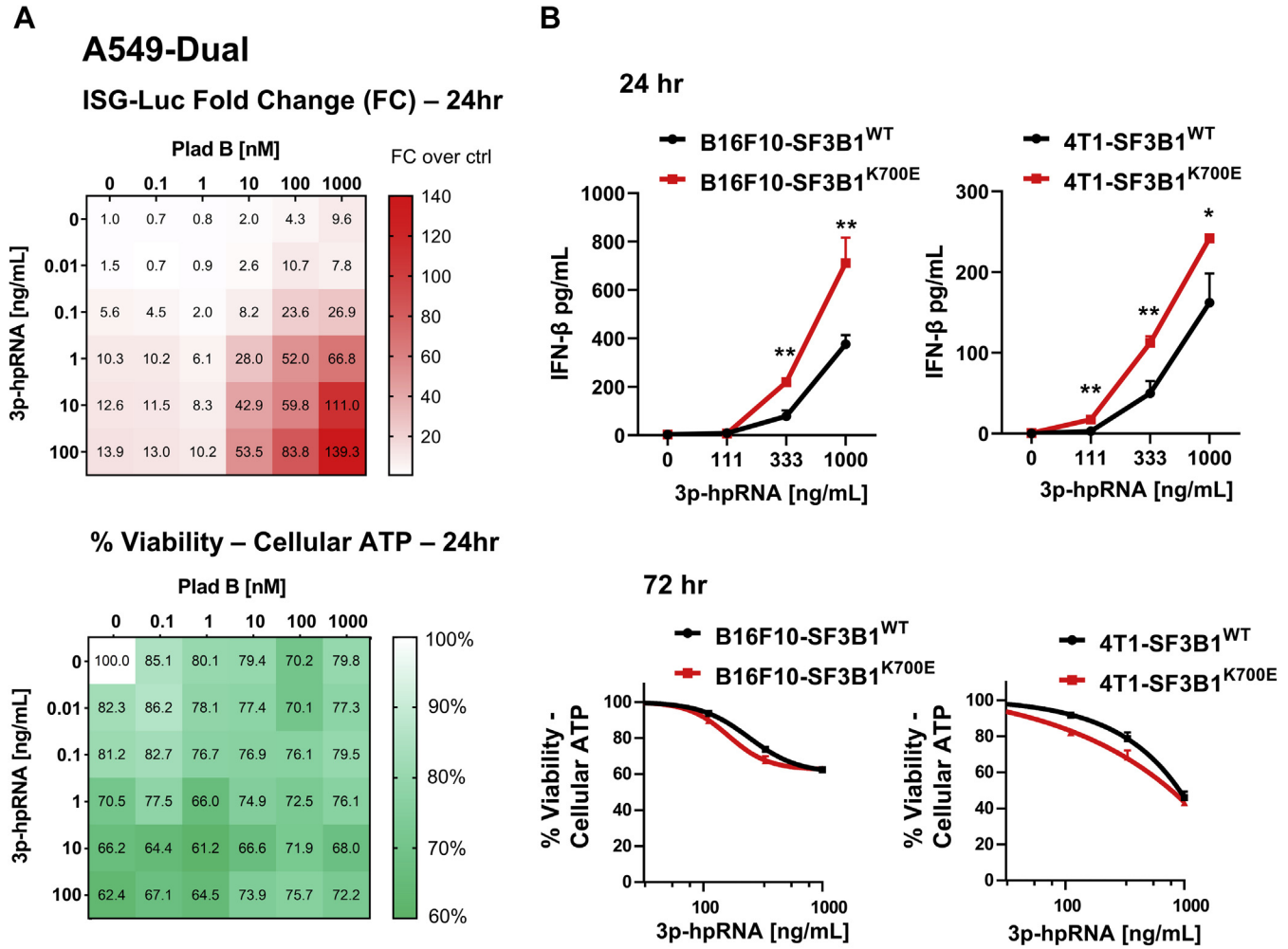


**Figure 5. SF3B1 modulator synergizes with RIG-I agonist for IFN-I response.** *A*, A549-Dual cells were treated for 24 h with varying doses of Plad B in combination with varying doses of the RIG-I agonist 3p-hpRNA. IFN-I response was quantified by QUANTI-Luc assay to determine ISG-LU. A heat map of fold change (FC) of ISG-Luc signal over control cells (untreated) is plotted along with percent of cell viabilities as measured by CellTiter-Glo. Average value of duplicate samples is shown. *B*, lentivirus-transduced SF3B1$^{WT}$ or SF3B1$^{K700E}$ cells were treated with 3p-hpRNA for 24 h, and IFN-β in the supernatant was measured by ELISA (*top panels*). 3p-hpRNA was not substantially cytotoxic at 24 h, and thus percent of cell viabilities at 72 h as measured by CellTiter-Glo are plotted (*bottom panel*). Statistical analyses were performed using the unpaired parametric *t* test comparing experimental samples to the relevant dose in control cells where indicated. *p* Values <0.05 were considered significant (*$p < 0.05$; **$p < 0.01$; ***$p < 0.001$; and ****$p < 0.0001$). All data are representative of n = 3 experiments. hpRNA, hairpin RNA; IFN-I, type I interferon; ISG, interferon-stimulated gene; LU, light unit; Plad B, pladienolide B; RIG-I, retinoic acid–inducible gene I; SF3B1, spliceosome splicing factor 3b subunit 1.

the unpredictable functions of mis-spliced neomorphic proteins. It is conceivable that during Plad B treatment, an alternatively spliced factor may gain structural homology to MAVS to have redundant function. However, this is speculation as current tools cannot predict such splice variant structure and function on a global scale.

An alternative postulation is that Plad B may initiate crosstalk with DNA-sensing pathways. Unlike healthy cells, cancer cells often accumulate cytoplasmic DNA from genomic and mitochondrial sources (39, 40). RNA-sensing pathways have substantial crosstalk with DNA-sensing pathways such as STING (41–43). A recent study suggests that epigenetic modulation induces cellular dsRNA species and expression of interferon-stimulated genes dependent on STING (44). Therefore, it is plausible that Plad B-mediated aberrant RNA species involve DNA-sensing pathways for IFN-I responses. Both RIG-I and DNA-sensing pathways converge on IRF3 activation and indeed, IRF3 was crucial for Plad B-mediated IFN-I responses. It is also reasonable to postulate that Plad B might generate cytoplasmic RNA:DNA hybrid molecules in cancer cells because of aberrant RNA species interacting with aberrant cytoplasmic DNA. Plad B induces cell cycle arrest (45, 46), which has been associated with cytoplasmic DNA leakage and activation of the cyclic GMP–AMP synthase–STING pathway (40, 47). RNA:DNA hybrid molecules in conjunction with ectopic cytoplasmic DNA might activate or recruit factors in DNA-sensing pathways, perhaps at the mitochondria, that cooperate with RIG-I to produce IFN-I. In this postulated model, RIG-I may primarily function as a scaffold for DNA-sensing pathway activation rather than actively signal on its own.

Finally, the data also suggest that SF3B1 modulators synergize well with canonical RIG-I agonists for IFN-I responses and that SF3B1-mutant cancers exhibit increased sensitivity to

a canonical RIG-I agonist for producing IFN-I. Plad B leads to antitumor cytotoxicity, whereas SF3B1$^{K700E}$ leads to neomorphic functions that are believed to be protumorigenic, thus they have seemingly opposite functions for cell viability. How two SF3B1 alterations with seemingly opposite functions converge on the RIG-I cascade is intriguing, and we offer potential hypotheses.

Both Plad B and SF3B1$^{K700E}$ lead to global aberrant RNA splicing (splicing inhibition, exon skipping, alternative branchpoint usage, etc.), and therefore, it is reasonable to believe that some alternatively spliced products may be shared. Some shared alternatively spliced RNA products, produced by both Plad B and SF3B1$^{K700E}$ mutation, may function as a RIG-I ligand. SF3B1$^{K700E}$ mutation may generate low levels of these ligands, insufficient to trigger spontaneous RIG-I signaling, but sufficient to increase RIG-I sensitivity to additional stimulation (such as 3p-hpRNA). In addition, SF3B1$^{K700E}$ neomorphic mutations are thought to be exclusively heterozygous in cancer because some level of WT SF3B1 function is required for cell viability (48). Therefore, SF3B1$^{K700E}$ neomorphic tumors have their basic cellular functions and viability sustained by the WT SF3B1 copy but have neomorphic and tumorigenic functions gained from the SF3B1$^{K700E}$ copy that lead to a net tumorigenic effect. In contrast, Plad B can modulate and disrupt essential functions of both SF3B1 copies and therefore has a net cytotoxic effect. This would be especially interesting to study in the context of MYC-driven tumors as MYC+ cancer cells are reported to have increased cytotoxic sensitivity to SF3B1 loss-of-function or pharmacological modulation (49).

It is interesting that although Plad B and 3p-hpRNA synergized for IFN-I response in A549 cells, they did not synergize for cytotoxicity. Plad B has been characterized to induce both cell-cycle arrest and apoptosis (19, 45, 46, 50). RIG-I agonists such as 3p-hpRNA have been characterized to induce apoptosis and pyroptosis. Plad B cytotoxicity does not depend on RIG-I expression and therefore is likely distinct from RIG-I-associated apoptosis pathways. Indeed, it is possible that during cotreatment of Plad B and 3p-hpRNA, Plad B can limit appropriate splicing of crucial factors in canonical RIG-I-mediated apoptosis. In addition, it is possible that Plad B preferentially induces cell cycle arrest in A549 cells rather than apoptosis and that this does not cooperate with RIG-I-mediated apoptosis at early time points. The data also suggest that autocrine IFN-I signaling is not important for Plad B-mediated cytotoxicity. It is likely that Plad B does not induce cell death through RIG-I pathway activation but rather disrupts basic cellular functions when splicing is globally impaired. It would also be interesting to better delineate the mechanisms of Plad B cytotoxic effects. For example, it is unclear whether Plad B induces pyroptosis.

It is necessary to consider that Plad B directly affects splicing and therefore likely affects appropriately spliced transcripts at higher doses. Therefore, it should not be expected that Plad B-induced responses follow the exact signature of canonical RIG-I signaling. Plad B could instead lead to a unique dose-responsive effect on certain induced factors. For example, IFN-β does not undergo splicing and indeed, IFN-β transcripts continue to increase with the dose of Plad B (Fig. 1*B*). However, ISG54 does require splicing, and ISG54 transcripts peak at 30 nM Plad B but then decline at 100 and 1000 nM. It is likely that at high doses of Plad B, although RIG-I-mediated promotion of ISG54 transcription is largely intact, the ISG54 transcripts themselves are being mis-spliced and degraded. This is not reflected in the A549-Dual ISG54 reporter because the exogenous ISG54 reporter transcript (Luciferase) presumably does not require splicing.

As SF3B1 modulators enter clinical trials based on cancer cytotoxicity data, we identify another potential role of these agents. SF3B1 modulator–induced IFN-I production in the tumor microenvironment may boost immune responses in addition to direct cytotoxic effects on tumor cells. In addition, other reports have suggested that SF3B1-mutant tumors may express more mis-spliced neoantigens that result from tumor-specific splice junctions, alternative isoform, and retained introns (15, 51). Neoantigen burden has been reported to correlate with response to immune checkpoint blockade (52). However, mis-spliced neoantigens would not be identified using common prediction methods that focus on somatic mutation–derived neoantigens. Although still unclear, mis-spliced neoantigens may contribute to the immunogenicity of SF3B1-mutant tumors (15). Indeed, a recent study has described shared splicing neoantigens derived from SF3B1-mutant uveal melanomas in patients (53). Therefore, it would be valuable to test the combination therapy of RIG-I agonists with checkpoint blockade in SF3B1-mutant tumors *in vivo*. This strategy would potentially enhance activation of both the innate and adaptive antitumor immune response.

## Experimental procedures

### Cell lines and viability assays

B16F10, CT26, 4T1, and MC38 murine lines were purchased from American Type Culture Collection, expanded, confirmed to be mycoplasma free, and then frozen as aliquots. HEK reporter lines, A549-Dual, and the derived genetic KO reporter lines were purchased from Invivogen: HEK-Lucia Null (hkl-null), HEK-Lucia RIG-I (hkl-hrigi), A549-Dual (a549d-nfis), A549-Dual-RIG-I-KO (a549d-korigi), A549-Dual-MDA5-KO (a549d-komda5), A549-Dual-MAVS-KO (a549d-komavs), THP1-Dual (thpd-nfis), THP1-Dual-IRF3-KO (thpd-koirf3), and THP1-Dual-MAVS-KO (thpd-komavs). All reporter cell lines from Invivogen were maintained as recommended by the manufacturer. Murine cell lines were maintained in American Type Culture Collection recommended media. Viability assays were performed using the CellTiter-Glo Luminescent Cell Viability Assay (Promega; G7573) following the manufacturer's instructions.

### CRISPR gene editing

For B16F10-SF3B1$^{R1074H}$ generation, an sgRNA, which cuts close to the desired edit, and an ssODN donor template with homology arms identical to the nontargeting strand and silent mutations in the PAM sequence were designed. CRISPR–Cas9 and homology-directed repair (HDR) reagents were obtained


ASBMB

from IDT. About 200,000 cells were nucleofected with ribonucleoprotein complexes containing 150 pmol gRNA and 125 pmol Cas9, 3 μM Ultramer ssODN donor template, and electroporation enhancer using SE solution and pulse code CM-150, in a final volume of 25 μl per sample in a 16-well Nucleocuvette strip (Lonza) following the manufacturers' protocols. Cells were then plated in two 96-well plates with 22.5 μM HDR enhancer (IDT). HDR enhancer was washed out after 12 to 24 h. About 48 h after nucleofection, half the cells were lysed for next-generation sequencing (NGS) and the other half of the cells were subjected to single-cell cloning. Single-cell clones were sequenced, and five clones with the identical SF3B1$^{R1074H}$ mutation were pooled and expanded further. B16F10 exhibits chromosomal aneuploidy. Sequencing data suggests five alleles of SF3B1. After CRISPR editing, each of the five clones contained the approximate allele frequency at the SF3B1 locus: 20% WT, 20% SF3B1$^{R1074H}$, and 60% INDEL. It was predicted and assumed that indel alleles would be degraded through nonsense-mediated decay. HDR template and sgRNA were as follows: SF3B1$^{R1074H}$ HDR template: ATTATAACCTACTCACCCAATAGCCTTTGCGATATAA CCAAATGTATTGACTGTAGCTCTGTGAATAGCTTTTT TGTGAGCTTTTAAGAGCTCTAAAAGCTCA. SF3B1-R10 74H sgRNA: GATATAACCAAATGTATTGA. For CT26-RIG-I-KO and B16F10-RIG-I-KO generation, cells were nucleofected as aforementioned using an sgRNA designed against murine RIG-I (DDX58) (CATGTAGCTGAGGATG TAGG) except without the HDR enhancer. Cells were subjected to single-cell cloning, confirmed by NGS, and clones were tested for successful KO through immunoblot and ELISA. For the additional A549-Dual-MAVS-KO clone generation, a pair of sgRNAs were designed to cut on either end of exon 2 of MAVS (sgRNAs: GGGAAGTGACAGCCCG ACAC and ACAGATCACACATTACAACA). A549-Dual (Invivogen; a549d-nfis) reporter cells were transfected using the Lipofectamine CRISPRMAX kit (Thermo Fisher Scientific; CMAX00008) with 25 pmol of each sgRNA (Synthego) and 6.25 μg TrueCut Cas9 (Thermo Fisher Scientific; A36496) in 6-well plates. Cells were subjected to single-cell cloning on the CellCelector (Automated Lab Solutions) into 96-well plates. Single-cell clones were confirmed by Sanger Sequencing and immunoblot with MAVS antibody (Abcam; catalog no. ab89825).

### SF3B1 modulator, 3p-hpRNA, and cytokine treatments

Plad B was purchased from Tocris (6070), and spliceostatin analog PF-06437837 (thailanstatin A methyl ester) was synthesized by Pfizer as previously reported (22). Cells were seeded in 96-well plates at 5000 cells/well (4T1), 10,000 cells/well (A549, CT26, and MC38 HEK), and 20,000 cells/well (B16F10) overnight in 75 μl media. The next day, 75 μl of a 2× solution of the indicated compound was added to wells, and cells were incubated at 37 °C until the indicated time points. Assays with THP1 cells were performed similarly except plating cells (100,000 cells) immediately before the addition of indicated compounds. Supernatant was removed and used in subsequent assays. 3p-hpRNA (Invivogen; tlrl-hprna) was prepared as a 2× solution in complex with the transfection reagent LyoVec (Invivogen; lyec-1) according to the manufacturer's instructions. After complexing, 75 μl of the 2× concentrated 3p-hpRNA/LyoVec was added to cells until the indicated time points. Positive control cytokines used were IFN-α2 (Biolegend; 592702) and TNFα (Biolegend; 570102).

### Immunoblots, chemokine measurements, ELISA, AlphaLISA, and reporter assays

Immunoblots (Western blots) were performed by extracting total cell lysate using radioimmunoprecipitation assay buffer (Thermo Fisher Scientific; 89900) with protease and phosphatase inhibitors (Thermo Fisher Scientific; 78440). Protein was quantified using the MicroBCA Protein Assay Kit (Thermo Fisher Scientific; 23235). Protein (20–30 μg) was loaded and run on Criterion 4–15% Tris–HCl gels (Bio-Rad; 345-0027 or 345-0028). After 1 h blocking with 5% bovine serum albumin at room temperature, immunoblotting was performed using the following primary antibodies overnight at 4 °C: Cell Signaling Technology; RIG-I (3743S: 1:1000 dilution), β-actin-horseradish peroxidase (5125S; 1:5000 dilution), IRF3 (11904S; 1:1000 dilution), and MAVS (24930S; 1:1000 dilution). Secondary antibodies were used by incubation of horseradish peroxidase–conjugated antibodies (Bio-Rad; 170-6515; 1:10,000 dilution) for 1 h at room temperature before washing and imaging using a myECL imager (Thermo Fisher Scientific). Antibodies used in Figure S4 are MAVS (abcam; catalog no. ab89825; 1:1000 dilution), anti-vinculin (abcam; catalog no. ab129002; 1:10,000 dilution), IRDye 800CW Goat antimouse (LI-COR; catalog no. 926-32210; 1:15,000 dilution), and IRDye 680RD Donkey anti-rabbit (LI-COR; catalog no. 926-68073; 1:15,000 dilution). Mouse chemokine measurements were performed using the MILLIPLEX MAP Mouse Cytokine/Chemokine Magnetic Bead Panel—Premixed 25 Plex —Immunology Multiplex Assay (Millipore; MCYTOMAG-70K-PMX). Human IL-6, IL-8, and TNFα were measured using human cytokine array/chemokine array 48-Plex (Eve Technologies; HD48). ELISAs were performed using supernatant following the manufacturer's instructions (Pestka Biomedical Laboratories; 42400-2 or 42410-2). IFN-β AlphaLISAs were performed using supernatant following the manufacturer's instructions (PerkinElmer; AL586C). IFN-I response reporter assays were performed using QUANTI-Luc (Invivogen; rep-qlc2), whereas NF-κB–SEAP assays were performed using QUANTI-Blue (Invivogen; rep-qb1) and following the manufacturer's instructions. For ISG-light unit (LU) fold change analysis, fold change was calculated a (experimental condition ISG-LU signal)/(dimethyl sulfoxide control ISG-LU signal). For THP-1 IFN-I response reporter assays, QUANTI-Luc signal was normalized to relative viability because of high sensitivity to Plad B-mediated cytotoxicity. Normalization was calculated as: (ISG-LU fold change)/(proportion of viable cells as measured by CellTiter-Glo Luminescent Cell Viability Assay) (Promega; G7573).

### Quantitative PCR and intron retention experiments

Quantitative PCR was performed using the TaqMan real-time PCR system. RNA was extracted using the Qiagen RNeasy Mini Plus kit (Qiagen; 74134), 1 μg of RNA was reverse transcribed into complementary DNA (cDNA) using Superscript VILO cDNA Synthesis Kit (Invitrogen; 11754050), and TaqMan probes and primers were designed from "assay-on-demand" gene expression products (Thermo Fisher Scientific). Primers were as follows: human IFNB1 (Hs01077958_s1; 4331182), human IFIT2/ISG54 (Hs01922738_s1; 4331182), and human GAPDH (Hs04420632_g1; 4331182). The results are presented as fold changes based on the differences of normalized Ct values compared with control samples, assuming optimal primer efficiency (standard $2^{-\Delta\Delta Ct}$ method). Intron retention assay was performed by using a 35-round standard RT–PCR as outlined in past reports. Primers were as follows: DNAJB1—Forward: GAACCAAAATCACTTTCCCCAAGGAAGG and Reverse: AATGAGGTCCCCACGTTTCTCGGGTGT; RIOK3—Forward: CCAGTGACCTTATGCTGGCTCAGAT and Reverse: GGTCTGTAGGGATCATCACGAGTA; and GAPDH—Forward: TGGTCACCAGGGCTGCTT and Reverse: AGCTTCCCGTTCTCAGCCTT. RT–PCR products were resolved on 2% E-Gel EX Agarose Gels (Invitrogen; G401002).

### Lentiviral overexpression

Lentiviral constructs expressing human RIG-I and murine $SF3B1^{WT}$ were purchased from GeneCopoeia (Vector pReceiver-Lv156). In brief, the construct contained the human RIG-I (GeneCopoeia; T0237), murine $SF3B1^{WT}$ (GeneCopoeia; Mm35243), or $SF3B1^{K700E}$ ORF driven by the EF1α promoter. Murine $SF3B1^{K700E}$ was custom-cloned by GeneCopoeia from the $SF3B1^{WT}$ construct (GeneCopoeia; Mm35243). The constructs contained a puromycin resistance gene, and puromycin (4 μg/ml for 5 days) was used to select transduced cells.

### siRNA experiments

siRNA was purchased from Thermo Fisher Scientific—Ambion *In Vivo* Pre-Designed siRNA Application Silencer Select (4457308). Catalog numbers for individual siRNAs were as follows: siRNA Neg: 4457287, siRNA IRF3-1: S7508, siRNA IRF3-2: S7509, siRNA MAVS-1: S33178, and siRNA MAVS-2: S33179. Cells were seeded in 6-well plates at 150,000 cells/well in antibiotic-free media. Cells were transfected for 72 h using Lipofectamine RNAiMAX Transfection Reagent (Thermo Fisher Scientific; 13778030) following the manufacturer's protocol. Cells were then harvested, and a fraction is used for immunoblot analysis to confirm target knockdown. Cells were replated into 96-well plates at 20,000 cells per well for 6 h before Plad B was added for the next 24 h. Supernatant was used in QUANTI-Luc (Invivogen; rep-qlc2) assays.

### Data and statistical analysis

Data were plotted using Prism 8 (GraphPad Software, Inc). Dose–response curves were generated by log-transforming the data and either using the log(agonist) *versus* response – variable slope or log(inhibitor *versus* response – variable slope) function in Prism 8. Values reported represent mean + standard deviation of triplicate values. Values are representative of two to five independent experiments (as described in the legends to the figures). Statistical analyses were performed using the unpaired parametric *t* test with *p* values <0.05 considered significant ($^{*}p < 0.05$; $^{**}p < 0.01$; $^{***}p < 0.001$; and $^{****}p < 0.0001$).

## Data availability

All data are contained within the article.

*Supporting information*—This article contains supporting information.

*Acknowledgments*—We thank Dr Brendan Veeneman for the mouse RIG-I-KO sgRNA sequence and Dr Jason Arroyo for developing the NGS protocol and assistance with NGS data analysis. We acknowledge Dr Robert Abraham and Dr Kenneth G. Geles for insightful discussion.

*Author contributions*—A. Y. C., Y.-M. W., P. M. L., F. L., and S.-R. W. conceptualization; A. Y. C., Y.-M. W., P. M. L., F. L., and S.-R. W. methodology; A. Y. C., Y. J. Z., Y.-M. W., and P. M. L. formal analysis; A. Y. C., Y. J. Z., S. I., P. W. P., P. T., K. M. S., and H. W. investigation; A. Y. C., Y. J. Z., S. I., P. W. P., P. T., K. M. S., H. W., Y.-M. W., and P. M. L. data curation; A. Y. C. writing–original draft; A. Y. C., Y. J. Z., S. I., Y.-M. W., P. M. L., F. L., and S.-R. W. writing–review and editing; F. L. and S.-R. W. supervision.

*Funding and additional information*—All studies were funded by Pfizer, Inc.

*Conflict of interest*—All authors were employees of Pfizer, Inc during the duration of this work.

*Abbreviations*—The abbreviations used are: cDNA, complementary DNA; HDR, homology-directed repair; HEK, human embryonic kidney; hpRNA, hairpin RNA; IFN-I, type I interferon; IL, interleukin; IRF3, interferon regulatory factor 3; ISG54, interferon-stimulated gene 54; LU, light unit; MAVS, mitochondrial antiviral signaling protein; MDA5, melanoma differentiation–associated protein 5; NGS, next-generation sequencing; Plad B, pladienolide B; RIG-I, retinoic acid–inducible gene I; SEAP, secreted embryonic alkaline phosphatase; SF3B1, spliceosome splicing factor 3b subunit 1; sgRNA, single-guide RNA; STING, stimulator of interferon genes; TNFα, tumor necrosis factor alpha.

## References

1. Loo, Y. M., and Gale, M. (2011) Immune signaling by RIG-I-like receptors. *Immunity* **34**, 680–692
2. Woo, S. R., Fuertes, M. B., Corrales, L., Spranger, S., Furdyna, M. J., Leung, M. Y. K., Duggan, R., Wang, Y., Barber, G. N., Fitzgerald, K. A., Alegre, M. L., and Gajewski, T. F. (2014) STING-dependent cytosolic DNA sensing mediates innate immune recognition of immunogenic tumors. *Immunity* **41**, 830–842
3. Lässig, C., and Hopfner, K. P. (2017) Discrimination of cytosolic self and non-self RNA by RIG-I-like receptors. *J. Biol. Chem.* **292**, 9000–9009

4. Yoneyama, M., and Fujita, T. (2007) Function of RIG-I-like receptors in antiviral innate immunity. *J. Biol. Chem.* **282**, 15315–15318
5. Elion, D. L., Jacobson, M. E., Hicks, D. J., Rahman, B., Sanchez, V., Gonzales-Ericsson, P. I., Fedorova, O., Pyle, A. M., Wilson, J. T., and Cook, R. S. (2018) Therapeutically active RIG-I agonist induces immunogenic tumor cell killing in breast cancers. *Cancer Res.* **78**, 6183–6195
6. Heidegger, S., Wintges, A., Stritzke, F., Bek, S., Steiger, K., Koenig, P. A., Göttert, S., Engleitner, T., Öllinger, R., Nedelko, T., Fischer, J. C., Makarov, V., Winter, C., Rad, R., Van Den Brink, M. R. M., *et al.* (2019) RIG-I activation is critical for responsiveness to checkpoint blockade. *Sci. Immunol.* **4**, eaau8943
7. Patel, S. A., and Minn, A. J. (2018) Combination cancer therapy with immune checkpoint blockade: Mechanisms and strategies. *Immunity* **48**, 417–433
8. Brown, J. S., Sundar, R., and Lopez, J. (2018) Combining DNA damaging therapeutics with immunotherapy: More haste, less speed. *Br. J. Cancer* **118**, 312–324
9. Pantelidou, C., Sonzogni, O., Taveira, M. D. O., Mehta, A. K., Kothari, A., Wang, D., Visal, T., Li, M. K., Pinto, J., Castrillon, J. A., Cheney, E. M., Bouwman, P., Jonkers, J., Rottenberg, S., Guerriero, J. L., *et al.* (2019) Parp inhibitor efficacy depends on CD8+ T-cell recruitment via intratumoral sting pathway activation in BRCA-deficient models of triple-negative breast cancer. *Cancer Discov.* **9**, 722–737
10. Ishizuka, J. J., Manguso, R. T., Cheruiyot, C. K., Bi, K., Panda, A., Iracheta-Vellve, A., Miller, B. C., Du, P. P., Yates, K. B., Dubrot, J., Buchumenski, I., Comstock, D. E., Brown, F. D., Ayer, A., Kohnle, I. C., *et al.* (2019) Loss of ADAR1 in tumours overcomes resistance to immune checkpoint blockade. *Nature* **565**, 43–48
11. Samuel, C. E. (2019) Adenosine deaminase acting on RNA (ADAR1), a suppressor of double-stranded RNA–triggered innate immune responses. *J. Biol. Chem.* **294**, 1710–1720
12. Chen, Y. G., Chen, R., Ahmad, S., Verma, R., Kasturi, S. P., Amaya, L., Broughton, J. P., Kim, J., Cadena, C., Pulendran, B., Hur, S., and Chang, H. Y. (2019) N6-Methyladenosine modification controls circular RNA immunity. *Mol. Cell.* **76**, 96–109.e9
13. Lee, S. C. W., and Abdel-Wahab, O. (2016) Therapeutic targeting of splicing in cancer. *Nat. Med.* **22**, 976–986
14. El Marabti, E., and Younis, I. (2018) The cancer spliceome: Reprograming of alternative splicing in cancer. *Front. Mol. Biosci.* **5**, 1–11
15. Obeng, E. A., Stewart, C., and Abdel-Wahab, O. (2019) Altered RNA processing in cancer pathogenesis and therapy. *Cancer Discov.* **9**, 1493–1510
16. Obeng, E. A., Chappell, R. J., Seiler, M., Chen, M. C., Campagna, D. R., Schmidt, P. J., Schneider, R. K., Lord, A. M., Wang, L., Gambe, R. G., McConkey, M. E., Ali, A. M., Raza, A., Yu, L., Buonamici, S., *et al.* (2016) Physiologic expression of Sf3b1 K700E causes impaired erythropoiesis, aberrant splicing, and sensitivity to therapeutic spliceosome modulation. *Cancer Cell* **30**, 404–417
17. Mupo, A., Seiler, M., Sathiaseelan, V., Pance, A., Yang, Y., Agrawal, A. A., Iorio, F., Bautista, R., Pacharne, S., Tzelepis, K., Manes, N., Wright, P., Papaemmanuil, E., Kent, D. G., Campbell, P. C., *et al.* (2017) Hemopoietic-specific Sf3b1-K700E knock-in mice display the splicing defect seen in human MDS but develop anemia without ring sideroblasts. *Leukemia* **31**, 720–727
18. Anczukow, O., and Krainer, A. R. (2016) Splicing-factor alterations in cancers. *RNA* **22**, 1285–1301
19. Kashyap, M. K., Kumar, D., Villa, R., La Clair, J. J., Benner, C., Sasik, R., Jones, H., Ghia, E. M., Rassenti, L. Z., Kipps, T. J., Burkart, M. D., and Castro, J. E. (2015) Targeting the spliceosome in chronic lymphocytic leukemia with the macrolides FD-895 and pladienolide-B. *Haematologica* **100**, 945
20. Seiler, M., Yoshimi, A., Darman, R., Chan, B., Keaney, G., Thomas, M., Agrawal, A. A., Caleb, B., Csibi, A., Sean, E., Fekkes, P., Karr, C., Klimek, V., Lai, G., Lee, L., *et al.* (2018) H3B-8800, an orally available small-molecule splicing modulator, induces lethality in spliceosome-mutant cancers. *Nat. Med.* **24**, 497–504
21. Salton, M., and Misteli, T. (2016) Small molecule modulators of pre-mRNA splicing in cancer therapy. *Trends Mol. Med.* **22**, 28–37
22. Puthenveetil, S., Loganzo, F., He, H., Dirico, K., Green, M., Teske, J., Musto, S., Clark, T., Rago, B., Koehn, F., Veneziale, R., Falahaptisheh, H., Han, X., Barletta, F., Lucas, J., *et al.* (2016) Natural product splicing inhibitors: A New class of antibody–drug conjugate (ADC) payloads. *Bioconjug. Chem.* **27**, 1880–1888
23. Cretu, C., Agrawal, A. A., Cook, A., Will, C. L., Fekkes, P., Smith, P. G., Lührmann, R., Larsen, N., Buonamici, S., and Pena, V. (2018) Structural basis of splicing modulation by antitumor macrolide compounds. *Mol. Cell.* **70**, 265–273.e8
24. Teng, T., Tsai, J. H., Puyang, X., Seiler, M., Peng, S., Prajapati, S., Aird, D., Buonamici, S., Caleb, B., Chan, B., Corson, L., Feala, J., Fekkes, P., Gerard, B., Karr, C., *et al.* (2017) Splicing modulators act at the branch point adenosine binding pocket defined by the PHF5A-SF3b complex. *Nat. Commun.* **8**, 1–16
25. Corrionero, A., Miñana, B., and Valcárcel, J. (2011) Reduced fidelity of branch point recognition and alternative splicing induced by the anti-tumor drug spliceostatin A. *Genes Dev.* **25**, 445–459
26. Liang, D., Tatomer, D. C., Luo, Z., Wu, H., Yang, L., Chen, L. L., Cherry, S., and Wilusz, J. E. (2017) The output of protein-coding genes shifts to circular RNAs when the pre-mRNA processing machinery is limiting. *Mol. Cell.* **68**, 940–954.e3
27. Bonnal, S., Vigevani, L., and Valcárcel, J. (2012) The spliceosome as a target of novel antitumour drugs. *Nat. Rev. Drug Discov.* **11**, 847–859
28. He, H., Ratnayake, A. S., Janso, J. E., He, M., Yang, H. Y., Loganzo, F., Shor, B., O'Donnell, C. J., and Koehn, F. E. (2014) Cytotoxic spliceostatins from Burkholderia sp. and their semisynthetic analogues. *J. Nat. Prod.* **77**, 1864–1870
29. Yokoi, A., Kotake, Y., Takahashi, K., Kadowaki, T., Matsumoto, Y., Minoshima, Y., Sugi, N. H., Sagane, K., Hamaguchi, M., Iwata, M., and Mizui, Y. (2011) Biological validation that SF3b is a target of the anti-tumor macrolide pladienolide. *FEBS J.* **278**, 4870–4880
30. House, I. G., Savas, P., Lai, J., Chen, A. X. Y., Oliver, A. J., Teo, Z. L., Todd, K. L., Henderson, M. A., Giuffrida, L., Petley, E. V., Sek, K., Mardiana, S., Gide, T. N., Quek, C., Scolyer, R. A., *et al.* (2020) Macrophage-derived CXCL9 and CXCL10 are required for antitumor immune responses following immune checkpoint blockade. *Clin. Cancer Res.* **26**, 487–504
31. Kaesler, S., Wölbing, F., Kempf, W. E., Skabytska, Y., Köberle, M., Volz, T., Sinnberg, T., Amaral, T., Möckel, S., Yazdi, A., Metzler, G., Schaller, M., Hartmann, K., Weide, B., Garbe, C., *et al.* (2019) Targeting tumor-resident mast cells for effective anti-melanoma immune responses. *JCI Insight* **4**, e125057
32. Ren, X., Linehan, M. M., Iwasaki, A., and Pyle, A. M. (2019) RIG-I selectively discriminates against 5′-monophosphate RNA. *Cell Rep.* **26**, 2019–2027.e4
33. Dunker, W., Ye, X., Zhao, Y., Liu, L., Richardson, A., and Karijolich, J. (2021) TDP-43 prevents endogenous RNAs from triggering a lethal RIG-I-dependent interferon response. *Cell Rep.* **35**, 108976
34. Chen, Y. G., Kim, M. V., Chen, X., Batista, P. J., Aoyama, S., Wilusz, J. E., Iwasaki, A., and Chang, H. Y. (2017) Sensing self and foreign circular RNAs by intron identity. *Mol. Cell.* **67**, 228–238.e5
35. Lin, H., Jiang, M., Liu, L., Yang, Z., Ma, Z., Liu, S., Ma, Y., Zhang, L., and Cao, X. (2019) The long noncoding RNA Lnczc3h7a promotes a TRIM25-mediated RIG-I antiviral innate immune response. *Nat. Immunol.* **20**, 812–823
36. Lee, S. C. W., North, K., Kim, E., Jang, E., Obeng, E., Lu, S. X., Liu, B., Inoue, D., Yoshimi, A., Ki, M., Yeo, M., Zhang, X. J., Kim, M. K., Cho, H., Chung, Y. R., *et al.* (2018) Synthetic lethal and convergent biological effects of cancer-associated spliceosomal gene mutations. *Cancer Cell* **34**, 225–241.e8
37. Poeck, H., Bscheider, M., Gross, O., Finger, K., Roth, S., Rebsamen, M., Hannesschläger, N., Schlee, M., Rothenfusser, S., Barchet, W., Kato, H., Akira, S., Inoue, S., Endres, S., Peschel, C., *et al.* (2010) Recognition of RNA virus by RIG-I results in activation of CARD9 and inflammasome signaling for interleukin 1β production. *Nat. Immunol.* **11**, 63–69
38. Smith, M. A., Choudhary, G. S., Pellagatti, A., Choi, K., Bolanos, L. C., Bhagat, T. D., Gordon-Mitchell, S., Von Ahrens, D., Pradhan, K., Steeples, V., Kim, S., Steidl, U., Walter, M., Fraser, I. D. C., Kulkarni, A., *et al.* (2019) U2AF1

mutations induce oncogenic IRAK4 isoforms and activate innate immune pathways in myeloid malignancies. *Nat. Cell Biol.* **21**, 640–650
39. Mohr, L., Toufektchan, E., von Morgen, P., Chu, K., Kapoor, A., and Maciejowski, J. (2021) ER-directed TREX1 limits cGAS activation at micronuclei. *Mol. Cell.* **81**, 724–738.e9
40. Takahashi, A., Loo, T. M., Okada, R., Kamachi, F., Watanabe, Y., Wakita, M., Watanabe, S., Kawamoto, S., Miyata, K., Barber, G. N., Ohtani, N., and Hara, E. (2018) Downregulation of cytoplasmic DNases is implicated in cytoplasmic DNA accumulation and SASP in senescent cells. *Nat. Commun.* **9**, 1249
41. Zevini, A., Olagnier, D., and Hiscott, J. (2017) Crosstalk between cytoplasmic RIG-I and STING sensing pathways. *Trends Immunol.* **38**, 194–205
42. Nazmi, A., Mukhopadhyay, R., Dutta, K., and Basu, A. (2012) STING mediates neuronal innate immune response following Japanese encephalitis virus infection. *Sci. Rep.* **2**, 347
43. Zhong, B., Yang, Y., Li, S., Wang, Y.-Y., Li, Y., Diao, F., Lei, C., He, X., Zhang, L., Tien, P., and Shu, H.-B. (2008) The adaptor protein MITA links virus-sensing receptors to IRF3 transcription factor activation. *Immunity* **29**, 538–550
44. Morel, K. L., Sheahan, A. V., Burkhart, D. L., Baca, S. C., Boufaied, N., Liu, Y., Qiu, X., Cañadas, I., Roehle, K., Heckler, M., Calagua, C., Ye, H., Pantelidou, C., Galbo, P., Panja, S., *et al.* (2021) EZH2 inhibition activates a dsRNA–STING–interferon stress axis that potentiates response to PD-1 checkpoint blockade in prostate cancer. *Nat. Cancer* **2**, 444–456
45. Effenberger, K. A., Anderson, D. D., Bray, W. M., Prichard, B. E., Ma, N., Adams, M. S., Ghosh, A. K., and Jurica, M. S. (2014) Coherence between cellular responses and *in vitro* splicing inhibition for the anti-tumor drug pladienolide b and its analogs. *J. Biol. Chem.* **289**, 1938–1947
46. Zhang, Q., Di, C., Yan, J., Wang, F., Qu, T., Wang, Y., Chen, Y., Zhang, X., Liu, Y., Yang, H., and Zhang, H. (2019) Inhibition of SF3b1 by pladienolide B evokes cycle arrest, apoptosis induction and p73 splicing in human cervical carcinoma cells. *Artif. Cells Nanomed. Biotechnol.* **47**, 1273–1280
47. Zierhut, C., Yamaguchi, N., Paredes, M., Luo, J.-D., Carroll, T., and Funabiki, H. (2019) The cytoplasmic DNA sensor cGAS promotes mitotic cell death. *Cell* **178**, 302–315. e23
48. Yoshida, K., Sanada, M., Shiraishi, Y., Nowak, D., Nagata, Y., Yamamoto, R., Sato, Y., Sato-Otsubo, A., Kon, A., Nagasaki, M., Chalkidis, G., Suzuki, Y., Shiosaka, M., Kawahata, R., Yamaguchi, T., *et al.* (2011) Frequent pathway mutations of splicing machinery in myelodysplasia. *Nature* **478**, 64–69
49. Hsu, T. Y.-T., Simon, L. M., Neill, N. J., Marcotte, R., Sayad, A., Bland, C. S., Echeverria, G. V., Sun, T., Kurley, S. J., Tyagi, S., Karlin, K. L., Dominguez-Vidaña, R., Hartman, J. D., Renwick, A., Scorsone, K., *et al.* (2015) The spliceosome is a therapeutic vulnerability in MYC-driven cancer. *Nature* **525**, 384–388
50. Jorge, J., Petronilho, S., Alves, R., Coucelo, M., Gonçalves, A. C., Nascimento Costa, J. M., and Sarmento-Ribeiro, A. B. (2020) Apoptosis induction and cell cycle arrest of pladienolide B in erythroleukemia cell lines. *Invest. New Drugs* **38**, 369–377
51. Frankiw, L., Baltimore, D., and Li, G. (2019) Alternative mRNA splicing in cancer immunotherapy. *Nat. Rev. Immunol.* **19**, 675–687
52. Keenan, T. E., Burke, K. P., and Van Allen, E. M. (2019) Genomic correlates of response to immune checkpoint blockade. *Nat. Med.* **25**, 389–402
53. Bigot, J., Lalanne, A. I., Lucibello, F., Gueguen, P., Houy, A., Dayot, S., Ganier, O., Gilet, J., Tosello, J., Nemati, F., Pierron, G., Waterfall, J. J., Barnhill, R., Gardrat, S., Piperno-Neumann, S., *et al.* (2021) Splicing patterns in SF3B1 mutated uveal melanoma generate shared immunogenic tumor-specific neo-epitopes. *Cancer Discov.* **11**, 1938–1951